Drop formation in viscous flows at a vertical capillary tube

D. F. Zhang and H. A. Stone
Division of Engineering & Applied Sciences, Harvard University, Cambridge, Massachusetts 02138

(Received 4 February 1997; accepted 14 April 1997)

Drop formation at the tip of a vertical, circular capillary tube immersed in a second immiscible fluid is studied numerically for low-Reynolds-number flows using the boundary integral method. The evolution and breakup of the drop fluid is considered to assess the influences of the viscosity ratio λ, the Bond number $\mathscr{B}$, and the capillary number $\mathscr{C}$ for $10^{-2} \leqslant \lambda \leqslant 10$, $10^{-2} \leqslant \mathscr{C} \leqslant 1$, and $0.1 \leqslant \mathscr{B} \leqslant 5$. For very small λ, breakup occurs at shorter times, there is no detectable thread between the detaching drop and the remaining pendant fluid column, and thus no large satellite drops are formed. The distance to detachment increases monotonically with λ and changes substantially for $\lambda > 1$, but the volume of the primary drop varies only slightly with λ. An additional application of the numerical investigation is to consider the effect of imposing a uniform flow in the ambient fluid [e.g., Oguz and Prosperetti, J. Fluid Mech. **257**, 111 (1993)], which is shown to lead to a smaller primary drop volume and a longer detachment length, as has been previously demonstrated primarily for high-Reynolds-number flows.
[S1070-6631(97)01808-4]

I. INTRODUCTION

Drop formation at the tip of a capillary tube occurs in a variety of engineering applications. Gases as well as liquids are commonly dispersed into a second fluid phase. Frequently cited applications include separation and extraction processes,[1] spraying and ink-jet printing technologies,[2] blood oxygenation,[3] and the bubble departure process during boiling (e.g., Ref. 4). A summary of many modeling ideas is provided by Clift *et al.*[5] from which it is clear that the majority of studies have concerned flows at high Reynolds numbers. Here we study the low-Reynolds-number situation by numerically investigating the detailed evolution of drop formation at the end of a capillary, continuing the simulations past breakup, in order to obtain insight into the formation of the primary drop and the largest satellite drop. Buoyancy, interfacial tension effects, viscous effects in both fluid phases, and the effect of an external flow are all considered.

When the flow rate is small, a static description of the shape of the drop is useful since a pendant droplet slowly forms at the capillary tip and the drop detaches when a critical volume is reached;[6–8] the critical volume corresponds to a balance between interfacial tension and buoyancy. These analyses have been modified to include dynamical effects and the primary focus of many studies has then been to predict the drop sizes as a function of the fluid properties, the nozzle geometry, and the flow rate inside the nozzle (e.g., Refs. 5 and 9). Conceptually, from a simplified modeling point of view, the drop formation process is conveniently divided into two stages: The first (nearly static) stage corresponds to growth of the drop attached to the capillary, which ends with a loss of equilibrium of forces, and the second stage corresponds to the necking and breaking of the drop. The final volume of the primary drop so formed is the sum of the volume of that portion of the static drop that breaks off at the end of the first stage and the volume that flows into the drop during the second, or pinching, stage. It should be noted that the predictions of these simplified models typically exhibit deviations from experimental measurements with errors exceeding 20%.[9,10]

Overall, two themes are common to the great majority of studies in this field. First, either gas-in-liquid (i.e., bubble formation) or liquid-in-gas (e.g., drops in air) systems have been investigated, where the gas has negligible dynamical influence; the complete two-phase flow situation has been seldom studied. Second, the majority of these dynamical studies have focused on inertial effects.[5] Hence we now summarize some recent studies of this drop formation problem with emphasis on investigations of viscous influences.

Wilson[11] developed a quasi-one-dimensional flow model to determine the drop volume formed by dripping from a fluid-filled tube into a gaseous surrounding. The flow is assumed to be a Stokes flow and the unsteady extension of the viscous thread as it sags under its own weight is analyzed. This useful model, however, is unable to describe flow near the nozzle exit, as well as the end of the thread, and an infinite detachment length is predicted. The predicted primary drop volume is about 25% lower than Wilson's own experiments. The viscous flow limit was also studied recently by Wong *et al.*[12] who investigated the formation of a bubble from a submerged capillary in a viscous environment. Numerical solutions in excellent agreement with their experiments were described.

A one-dimensional model for jet-like flows (liquid into gas) was presented recently by Eggers and DuPont.[13] These authors derived one-dimensional mass conservation and axial momentum equations accounting for viscous effects, inertia and capillarity by systematically approximating the Navier–Stokes equations. These ideas were applied to the highly nonlinear problem of pinching (breakup) of a fluid thread[14] and the model predictions were shown to be in excellent agreement with experiments focusing on the dynamics near breakup.[15–17] The breakup of the liquid thread shows a self-similar behavior during the final stages of the pinching

 1070-6631/97/9(8)/2234/9/$10.00

process where the flow near the exit has no influence. In particular, after the formation of a long thread with a nearly conical tip connected to an almost spherical drop, a remarkable series of smaller necks with thinner diameters were sequentially spawned. Following breakup and formation of a large primary drop, there is recoil of the liquid thread, and then secondary necking and breakup, which leads to satellite drops. The purely flow viscous limit of the pinching process was studied by Papageorgiou[18] (see also Ref. 19). This research, and many of its extensions, are described in a recent review article by Eggers.[20]

Recent investigations have utilized modern numerical methods to investigate the complete free-boundary problem in both the high- and low-Reynolds-number flow limits. For example, Oguz and Prosperetti[21] (see also Day and Hinch[22]) studied dynamics of bubble growth and detachment from a submerged needle by assuming the flow was inviscid and irrotational. A boundary integral method was used and several simple, illustrative models of the detachment process were developed. The boundary-integral numerical results were in excellent agreement with published experiments[23] as well as their own experiments. Oguz and Prosperetti also showed that bubbles growing when there is a liquid flowing parallel to the needle may detach with a considerably smaller radius than in a quiescent liquid (see also Clift *et al.*[5]). This significant effect motivated our investigation (Sec. III) of the analogous viscous flow problem. Also, in the spirit of Oguz and Prosperetti's numerical investigation of the free-boundary problem, Wong *et al.*[12] used a boundary integral method for low-Reynolds-number flows to study bubble detachment in a viscous fluid. Our work reported here thus combines elements of the above two investigations.

It is important to note that the aforementioned studies pertain to two limits of the drop formation processes: one is a liquid flowing into an ambient gas and the other is a gas ejected into a liquid. Here we explore the details of drop formation at a capillary in a general two-fluid system for a viscously dominated flow. Numerical results are based on the boundary integral method for Stokes flows. The formation, extension, and breakup of the drop fluid and, subsequently, the generation of satellite drops, are investigated for a wide range of fluid viscosity ratios. Other effects such as buoyancy, interfacial tension, and an external flow are also studied. We describe the numerical formulation in Sec. II and report numerical results in Sec. III.

II. NUMERICAL FORMULATION

The formation of a drop at the tip of a vertical, circular capillary tube of radius R_0 is shown in Fig. 1. An incompressible, Newtonian fluid ($i=1$) flows, owing to a pressure gradient, with a constant flow rate Q into a second incompressible, Newtonian fluid ($i=2$). For simplicity, the tube wall is assumed to have zero thickness, which is physically reasonable since the wall thickness has been shown experimentally to have little influence on the drop formation process.[24] The ambient fluid may be quiescent or may be assumed to be in a constant steady motion $\mathbf{U}_\infty$ far from the capillary; the latter case is representative of configurations where the characteristic dimension of the capillary is much smaller than the typical dimension over which the bulk flow varies. For this axisymmetric flow, a cylindrical coordinate system (r,z) is defined with the z axis coincident with that of the capillary tube, increasing in the direction of $\mathbf{g}$, and the origin is placed at the center of the tube exit (see Fig. 1).

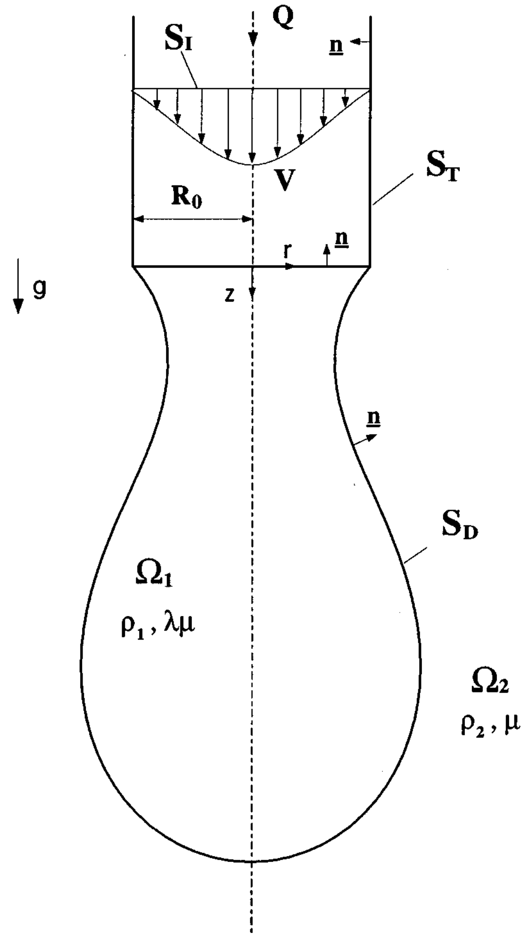

FIG. 1. Schematic of drop formation at a vertical, circular capillary tube.

In the low-Reynolds-number flow limit, the governing equations for motion of the two fluids are ($i=1,2$)

$$\nabla \cdot \mathbf{T}_i = -\nabla p_i + \mu_i \nabla^2 \mathbf{u}_i + \rho_i \mathbf{g} = \mathbf{0}, \quad \nabla \cdot \mathbf{u}_i = 0, \tag{1}$$

where in fluid i, $\mathbf{u}_i$ is the velocity field, p_i is the pressure, and μ_i and ρ_i are the fluid viscosity and density, respectively. In (1) the stress tensor $\mathbf{T}$ is defined to include the hydrostatic body force in order to define a divergence-free field,

$$\mathbf{T}_i = -(p_i - \rho_i \mathbf{g}\cdot\mathbf{x})\mathbf{I} + \mu_i(\nabla \mathbf{u}_i + (\nabla \mathbf{u}_i)^T), \tag{2}$$

where $\mathbf{x}$ is a position vector and $\mathbf{g}\cdot\mathbf{x} = gz$.

In the present study, the drop fluid ($\mathbf{x} \in \Omega_1$) is bounded by the fluid interface S_D, the capillary tube inner wall S_{T1}, and the tube inlet S_I. The ambient fluid ($\mathbf{x} \in \Omega_2$) is bounded internally by the fluid interface S_D and the capillary tube outer wall S_{T2}. In Fig. 1 these surfaces are represented by their traces in the (r,z) plane.

Inside the capillary tube, far from the tube exit, a Poiseuille flow is assumed and, thus, the velocity profile at the inlet S_I is

$$\mathbf{u}_1=\frac{2Q}{\pi R_0^2}\left[1-\left(\frac{r}{R_0}\right)^2\right]\mathbf{e}_z=2V\left[1-\left(\frac{r}{R_0}\right)^2\right]\mathbf{e}_z, \tag{3}$$

where $\mathbf{e}_z$ is the unit vector along the axis and V is the average fluid velocity in the capillary ($V=Q/\pi R_0^2$).

The boundary conditions along the inner and outer tube walls, S_{T1} and S_{T2}, are no slip: $\mathbf{u}_1=\mathbf{0}$, $\mathbf{u}_2=\mathbf{0}$. Along the fluid interface, S_D, the velocity is continuous, $\mathbf{u}_1=\mathbf{u}_2$, and the stress jump is balanced by the density contrast and the interfacial tension stress, which depends on the local curvature $\nabla_s\cdot\mathbf{n}$ of the interface,

$$\mathbf{n}\cdot\mathbf{T}_2-\mathbf{n}\cdot\mathbf{T}_1=[\gamma(\nabla_s\cdot\mathbf{n})-\Delta\rho\mathbf{g}\cdot\mathbf{x}]\mathbf{n}, \tag{4}$$

where γ is the constant interfacial tension, $\mathbf{n}$ is the unit normal vector directed into the ambient fluid, $\nabla_s=(\mathbf{I}-\mathbf{nn})\cdot\nabla$ is the gradient operator tangent to the interface, and $\Delta\rho=\rho_1-\rho_2$. Along S_D there is also a kinematic constraint, which can be expressed with the Lagrangian description of a labeled point $\mathbf{x}_L$ as

$$\frac{d\mathbf{x}_L}{dt}=\mathbf{u}(\mathbf{x}_L)\ \text{for}\ \ \mathbf{x}_L\in S_D. \tag{5}$$

The governing equations and boundary conditions are nondimensionalized by choosing the tube radius R_0 as the length scale, and it is convenient to choose the velocity scale as γ/μ. Accordingly, the scales for time and pressure, respectively, are $R_0\mu/\gamma$ and γ/R_0.

Three dimensionless parameters, a Bond number $\mathscr{B}$, a capillary number $\mathscr{C}$, and a viscosity ratio λ, describe the flow:

$$\mathscr{B}=\frac{\Delta\rho g R_0^2}{\gamma},\quad \lambda=\frac{\mu_1}{\mu_2},\quad \text{and}\ \ \mathscr{C}=\frac{\mu V}{\gamma}. \tag{6}$$

The Bond number measures the relative importance of the buoyancy force to the interfacial tension force while the capillary number represents the relative importance of the viscous force generated by the internal flow relative to the interfacial tension force. If a constant velocity $\mathbf{U}_\infty$ is imposed in the fluid surrounding the capillary, the outer capillary number $\mathscr{C}_{\text{out}}=\mu U_\infty/\gamma$ enters the problem description.

In order to solve this free-boundary problem, Stokes equations are reformulated into a system of integral equations. The numerical procedure is standard and the details can be found elsewhere.[25,26] In the present flow, along the tube walls the velocities $\mathbf{u}_1$ ($\mathbf{x}\in S_{T1}$) and $\mathbf{u}_2$ ($\mathbf{x}\in S_{T2}$) are identically zero, at the inlet S_I the velocity distribution is specified, and along the deforming fluid–fluid interface S_D the stress jump condition $(\mathbf{n}\cdot\mathbf{T}_2-\mathbf{n}\cdot\mathbf{T}_1)$ is known [Eq. (4)]. The unknown quantities are then $\mathbf{u}$ on S_D, $\mathbf{n}\cdot\mathbf{T}_1$ on S_{T1}, and $\mathbf{n}\cdot\mathbf{T}_2$ on S_{T2}; in fact, only the difference $(\mathbf{n}\cdot\mathbf{T}_2-\mathbf{n}\cdot\mathbf{T}_1)$ appears at the (infinitely thin) tube wall, S_T ($=S_{T1}=S_{T2}$). The final form of the boundary integral equations are

$$\begin{aligned}\frac{(1+\lambda)}{2}\mathbf{u}(\mathbf{x})=&\ \mathscr{C}_{\text{out}}\mathbf{e}_z+\int_{S_D}\mathbf{J}\cdot\mathbf{n}[(\nabla_s\cdot\mathbf{n})-\mathscr{B}z]dS_y+(\lambda-1)\\&\times\int_{S_D}\mathbf{n}\cdot\mathbf{K}\cdot\mathbf{u}\ dS_y+\int_{S_I}\mathbf{J}\cdot\mathbf{n}\cdot\mathbf{T}_1\ dS_y\\&+\lambda\int_{S_I}\mathbf{n}\cdot\mathbf{K}\cdot\mathbf{u}_1\ dS_y+\int_{S_T}\mathbf{J}\cdot(\mathbf{n}\cdot\mathbf{T}_2\\&-\mathbf{n}\cdot\mathbf{T}_1)dS_y\quad\text{for}\ \ \mathbf{x}\in S_D,\end{aligned} \tag{7a}$$

$$\begin{aligned}\mathbf{0}=&\ \mathscr{C}_{\text{out}}\mathbf{e}_z+\int_{S_D}\mathbf{J}\cdot\mathbf{n}[(\nabla_s\cdot\mathbf{n})-\mathscr{B}z]dS_y+(\lambda-1)\\&\times\int_{S_D}\mathbf{n}\cdot\mathbf{K}\cdot\mathbf{u}\ dS_y+\int_{S_I}\mathbf{J}\cdot\mathbf{n}\cdot\mathbf{T}_1\ dS_y+\lambda\int_{S_I}\mathbf{n}\cdot\mathbf{K}\cdot\mathbf{u}_1\ dS_y\\&+\int_{S_T}\mathbf{J}\cdot(\mathbf{n}\cdot\mathbf{T}_2-\mathbf{n}\cdot\mathbf{T}_1)dS_y,\quad\text{for}\ \ \mathbf{x}\in S_T,\end{aligned} \tag{7b}$$

where the kernels functions are

$$\begin{aligned}\mathbf{J}&=\frac{1}{8\pi}\left[\frac{\mathbf{I}}{|\mathbf{x}-\mathbf{y}|}+\frac{(\mathbf{x}-\mathbf{y})(\mathbf{x}-\mathbf{y})}{|\mathbf{x}-\mathbf{y}|^3}\right],\\\mathbf{K}&=-\frac{3}{4\pi}\frac{(\mathbf{x}-\mathbf{y})(\mathbf{x}-\mathbf{y})(\mathbf{x}-\mathbf{y})}{|\mathbf{x}-\mathbf{y}|^5}.\end{aligned} \tag{8}$$

We note that the capillary number appears in the dimensionless form of the inlet velocity profile (integral over S_I). For this axisymmetric flow, the surface integrals are simplified to line integrals along the generating curve of the boundary by performing the azimuthal integrations analytically.[27] Details of the numerical implementation are given in the Appendix and here we only note that although the drop was pinned at the edge of the tube, no contact angle was specified and so was allowed to take any value consistent with the numerical solution (e.g., Ref. 12).

III. RESULTS AND DISCUSSION

In this section the formation, extension, and breakup of the drop fluid and, subsequently, the generation of satellite drops, are investigated. Calculations are performed by varying one dimensionless parameter while keeping the other two parameters fixed and we have investigated $10^{-2}\leqslant\lambda\leqslant 10$, $10^{-2}\leqslant\mathscr{C}\leqslant 1$, and $0.1\leqslant\mathscr{B}\leqslant 5$. We have chosen to consider situations where the flow rate Q is fixed (constant $\mathscr{C}$), which, owing to the dynamics of interfacial rearrangement, would, in practice, require a time-varying pressure gradient. In common circumstances, this pressure change is not significant.[5]

For low-Reynolds-number flow situations, dimensional analysis implies, for example, that in the absence of an imposed flow in the external fluid the dimensionless volume V_d of the primary drop formed is $V_d=f(\mathscr{B},\mathscr{C},\lambda)$. In the nearly static limit, $\mathscr{C}\ll 1$, then $V_d\propto\mathscr{B}^{-1}$ for all λ.[8] However, although there have been many studies on bubble formation under high-Reynolds-number flow conditions, there appears

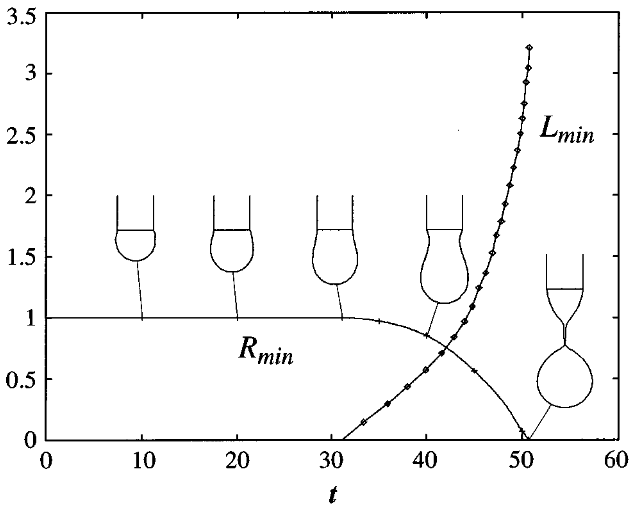

FIG. 2. Variation of the minimum dimensionless drop radius, R_{min}, and the corresponding dimensionless length, L_{min}, with time; $\lambda=0.1$, $\mathscr{B}=0.5$, and $\mathscr{C}=0.1$. Some drop shapes are also shown.

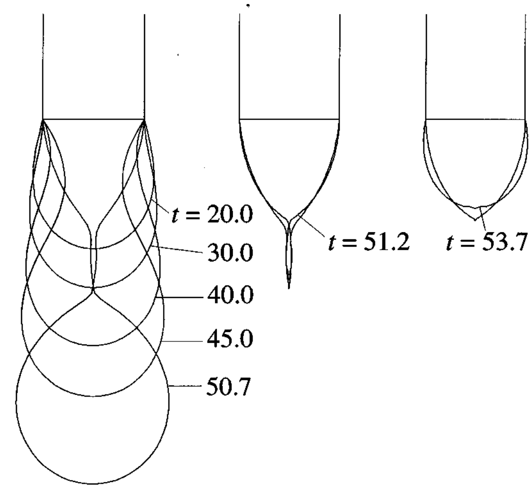

FIG. 3. A time sequence of the interface shapes for $\lambda=0.1$, $\mathscr{B}=0.5$, and $\mathscr{C}=0.1$. After separation of the primary and satellite drops from the main fluid column, the drops are neglected in further calculations of the pendant drop shape.

to be little specific information available about drop formation in viscous fluid flows[5] so our results for a wide range of $\mathscr{C}$, λ, and $\mathscr{C}_{\mathrm{out}}$ essentially are graphical forms of the dimensionless function f, or its analogue for other properties, for such parameters as the dimensionless drop volume, breaking time, and fluid column length at breakup.

A. Typical case

We first consider a typical case $\lambda=0.1$, $\mathscr{B}=0.5$, and $\mathscr{C}=0.1$. Figure 2 shows the variation of R_{min} and L_{min} with time, where R_{min} denotes the minimum dimensionless drop radius and L_{min} is the axial (z) distance from the capillary tube exit ($z=0$) to R_{min}. These two quantities characterize the formation of a neck which leads to breakup at a time t_b. Some drop shapes have also been included in Fig. 2. In the present numerical simulation, the drop is assumed to rupture, forming the primary drop, where $R_{\mathrm{min}}\leqslant 0.005$, which appears to be a reasonable numerical criterion for breakup when focus is on the primary drop since any additional decrease in the neck radius happens quickly and further computations of the solution become difficult because of the large velocity and curvature gradients near the pinch point (see, for example, Eggers[13] and Papageorgiou[18]). In fact, for a purely viscous internal (Stokes) flow, inertial effects become important as (rapid) pinching occurs,[18] so locally the low-Reynolds-number approximation becomes invalid. With an outer fluid present, however, the pinching dynamics are slowed and the low-Reynolds-number approximation can remain valid all the way to breakup.[28]

In Fig. 2 we observe that at early times, the drop volume increases by the continuous addition of fluid from the capillary tube and the interface shape transforms slowly from the hemispherical initial shape to a pear-shaped surface. During this period, the buoyancy force acting on the drop, which is proportional to the drop volume, is not large enough to overcome the interfacial tension force, and the drop remains attached to the capillary tube. Figure 2 shows that $R_{\mathrm{min}}=1$ and $L_{\mathrm{min}}=0$ for $t<30.2$, after which the drop volume reaches a critical value, predicted approximately by static stability analyses applicable to low capillary number flows, where the drop begins to break away (e.g., Middleman;[8] see also Fig. 9).

In order to distinguish the flow characteristics at different times, the drop formation process is generally divided into (at least) two stages, the latter stage after the drop begins to break away and is much shorter than the former. As a result of the rapid flow in the second stage, the drop stretches and a neck subsequently forms ($t\approx 40$). A thread then develops with a diameter that decreases rapidly with time. The shape of the thread is not symmetric about its horizontal centerline. The thread is connected to a nearly spherical primary drop at its lower end, where large curvatures develop and a local interfacial-tension-driven flow leads to breakup. At $t=50.7$, thread breakoff is about to occur with $L_{\mathrm{min}}\approx 3.16$. We note that the portion of the drop below the breaking point takes a spherical shape while the upper part approximates a cone (e.g., Peregrine *et al.*[17]). These shape features near pinching are common to most, if not all, examples of drop breakup and so from now on we focus on features of the shape and flow specific to drops formed at a capillary tube.

In order to demonstrate the entire drop formation process, in Fig. 3 a time sequence is shown (using the same parameters as in Fig. 2) including breakup of a drop, formation of a satellite drop, and return of the fluid interface to a blob-like shape similar to the initial shape. Growth, extension, necking, and breakup of the drop can be clearly seen prior to $t=50.7$. Immediately after the thread breaks at its lower end, its free end is retracted by interfacial tension. The thread breaks again at its upper end, resulting in the production of a small satellite droplet, as shown in Fig. 3 at $t=51.2$. Satellite drop formation depends primarily on the shape of the thread when it is about to break for the first time and so depends upon the initial and flow conditions (i.e., λ, $\mathscr{C}$, and $\mathscr{B}$); the volumes of the primary and satellite drops

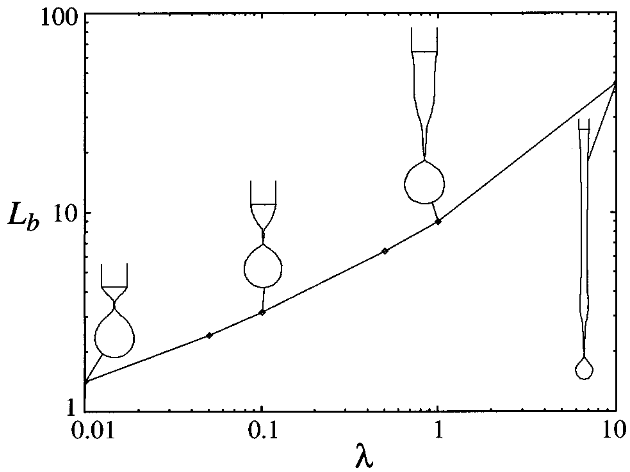

FIG. 4. The breaking length L_b versus λ for $\mathscr{B}=0.5$ and $\mathscr{C}=0.1$. Four shapes of the fluid interfaces at breakup are included for $\lambda=10^{-2}, 10^{-1}$, 1, and 10, respectively. The drop shape shown for $\lambda=10$ is displayed with compressed horizontal and vertical scales since very long fluid columns develop for $\lambda \gg 1$.

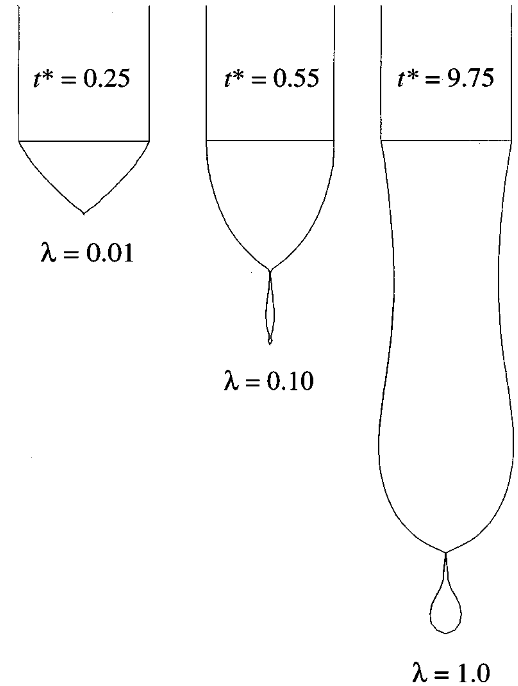

FIG. 5. The fluid interfaces for $\lambda=10^{-2}$, 10^{-1}, and 1 at the instant of the primary satellite drop detachment with $\mathscr{B}=0.5$, $\mathscr{C}=0.1$. The viscosity ratio λ and the satellite drop formation time $t^*=t-t_b$ are labeled on the figures.

are studied in the remaining sections. After a complete breakup process, leading to the formation of primary and satellite drops, the remaining drop fluid which hangs on the tube continues to deform and subsequently, another similar drop formation process occurs. Careful examination shows that the interface shape at $t=53.7$ is almost identical to that at $t=10.0$ (see Fig. 2).

B. Effect of the viscosity ratio λ

The viscosity ratio λ plays an important role during the dynamical processes of necking and breaking. Figure 4 shows the breaking length L_b versus λ for $\mathscr{B}=0.5$ and $\mathscr{C}=0.1$, where L_b is the dimensionless axial (z) location of the breaking point. Four interface shapes, just prior to breakoff, have also been included. The interface shapes for $\lambda=10^{-2}$, 10^{-1}, 1 are displayed with the same scale while that for $\lambda=10$ is presented with a much smaller scale owing to the very long fluid column that is formed for this large viscosity ratio. Clearly, as λ varies, there are different shapes at breakup and although, as we shall see, the primary drop volume changes only a little with λ for the range of $\mathscr{C}$ and $\mathscr{B}$ studied, the viscosity ratio has a significant effect on the formation of satellites. For $\lambda=10^{-2}$ breakup occurs at an early time, there is no detectable thread between the detaching drop and the remaining pendant drop, and so no large satellite drops are expected. This interface shape, calculated for a low value of the capillary number, is similar to that calculated for bubbles in Stokes flows by Wong *et al.*[12] and observed experimentally by Longuet-Higgins *et al.*[23] and experimentally and numerically by Oguz and Prosperetti[21] during the high-Reynolds-number bubble formation process from a needle ($\lambda \to 0$); dynamics (viscous or inertial) only play a significant role at late times near pinching. As λ is increased, a fluid thread develops and its length increases owing primarily to the difficulty of fluid squeezing out axially along the thread. Thus viscous effects play a significant role when threads form as breakup occurs. As a result, the breaking distance L_b increases monotonically with λ and rather dramatically for $\lambda>1$.

As indicated in the introduction, long, narrow threads which connect the falling drop and the remaining fluid column have been experimentally and theoretically observed in previous studies of high-viscosity dripping flows,[11,13,15,24] with much recent interest given to the dynamics in the neighborhood of the pinch point.[19,20] The consistency of the present results with these previous studies is not surprising since in fact these previous studies are an asymptotic limit ($\lambda \to \infty$) of the two-fluid flow. We note that numerical accuracy in the calculations presented here is difficult to preserve for the very extended interface shapes characteristic of $\lambda \gg 1$, as large numbers of node points must be used, and this requirement limited our calculations to $\lambda \leqslant 10$. Also, detailed investigations of the dynamics near pinching shows that, in fact, inertia eventually becomes important if $\lambda=\infty$ but can remain insignificant for the finite λ case.[28]

The viscosity ratio also influences formation of satellite drops. Figure 5 depicts the interfaces for $\lambda=10^{-2}$, 10^{-1}, 1 at the instant of the satellite drop detachment ($\mathscr{B}=0.5$ and $\mathscr{C}=0.1$). Satellites form for $\lambda=10^{-1}$ and 1 but, for $\lambda=10^{-2}$, there exists no visible thread, thus no satellite drop is expected. For $\lambda=10^{-1}$, a thin thread evolves and the breakup of this thread occurs soon after formation of the primary drop, ($t^*=t-t_b=0.55$), which generates a very small satellite ($V_s=5.6\times10^{-3}$). In contrast, relatively slow satellite drop formation occurs for $\lambda=1$ ($t^*=9.75$) and the satellite drop ($V_s=8\times10^{-2}$) is larger than that for $\lambda=10^{-1}$, a result which is due to the existence of the longer thread in the case of the more viscous drop fluid.

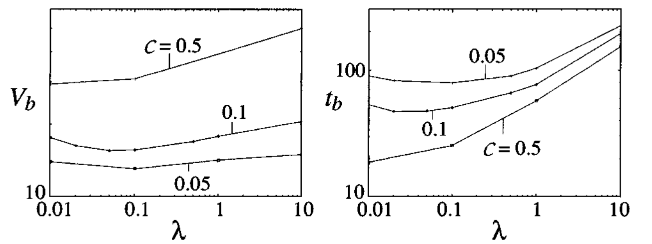

FIG. 6. The dimensionless breaking time t_b and the dimensionless volume of the primary drop V_b as a function of λ for $\mathscr{B}=0.5$ and $\mathscr{C}=5\times10^{-2}$, 10^{-1}, and 5×10^{-1}, respectively.

Figures 6 summarizes the dimensionless breaking times (t_b) and the dimensionless volumes of the primary drop (V_b). The Bond number is maintained constant ($\mathscr{B}=0.5$) and three capillary numbers ($\mathscr{C}=0.05,0.1$, and 0.5) are considered, corresponding to an increasing pressure difference driving larger flow rates through the tube. We note that V_b varies only a little as λ varies, especially for the small capillary number cases, e.g., $\mathscr{C}=0.05$, in spite of the different dynamics indicated in Fig. 4, and so static predictions, dependent on the Bond number, for the primary drop volume will be useful. Viscous stresses are more important as the capillary number increases, and correspond to shorter breaking times and larger primary drop volumes. Also, the viscosity ratio influences the flow during the latter stages, which terminate in breakup with different breaking lengths L_b (Fig. 4) and breaking times t_b (Fig. 6).

C. Effect of the Bond number $\mathscr{B}$

The effect of the Bond number is demonstrated in Fig. 7 for $0.1\leqslant\mathscr{B}\leqslant5$ with $\lambda=0.1$ and $\mathscr{C}=0.1$. Three interface shapes at breakup are shown for $\mathscr{B}=0.1$, 1, and 5, respectively. The primary drop volume V_b decreases nearly linearly with $\mathscr{B}$, and our numerical results indicate that $V_b\propto\mathscr{B}^{-n}$ with $n\approx0.90$, which is similar to theoretical results based upon a static analysis[8] for which the critical drop radius is

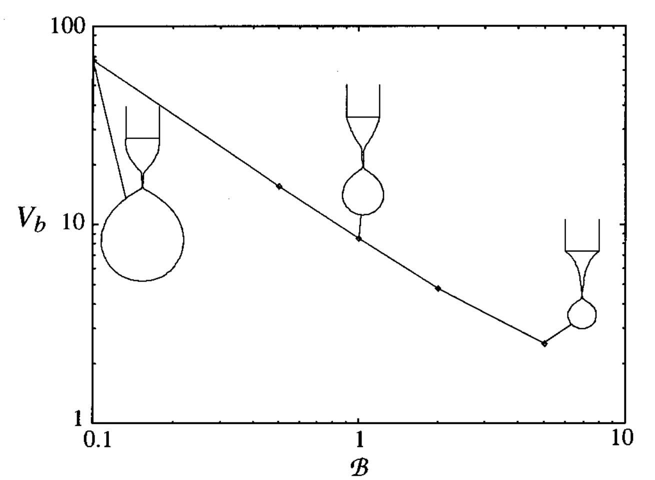

FIG. 7. Variation of the primary drop volume V_b with $\mathscr{B}$; $\lambda=0.1$, $\mathscr{C}=0.1$. The interface shapes at breakup for $\mathscr{B}=0.1$, 1, and 5 are also shown.

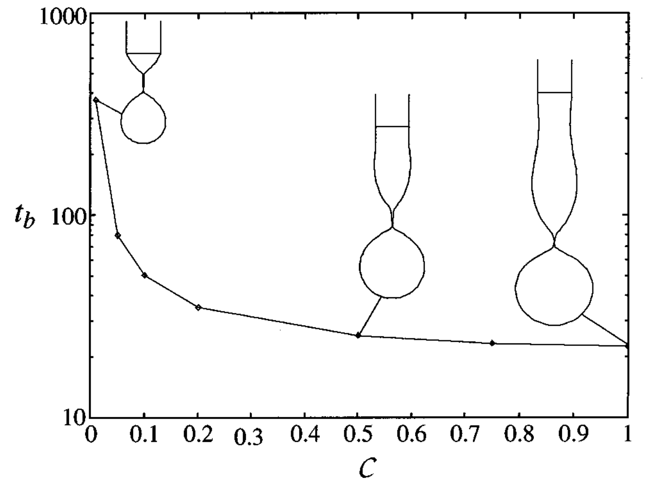

FIG. 8. Variation of t_b as a function of the capillary number $\mathscr{C}$; $\mathscr{B}=0.5$ and $\lambda=0.1$.

$R_d=(3\gamma/16R_0^2\rho g)^{1/3}$, where the released drop is assumed to be a sphere; nondimensionalization gives $R_d/R_0\propto\mathscr{B}^{-1/3}$ or $V_b\propto\mathscr{B}^{-1}$. The small deviation of the exponent n from unity is attributed to the small but finite capillary number as well as the viscous dynamics at later times.

Referring again to Fig. 7, we note that for larger Bond numbers, e.g., $\mathscr{B}=5$, substantial translation of the drop occurs on a short time scale which effectively leads to formation of narrow, tapered threads connecting the drop and fluid column. Further calculations show that the dynamics of the subsequent satellite formation for varying $\mathscr{B}$ are also different because the thread shape is substantially changed. For small $\mathscr{B}$ (= 0.1), a small satellite relative to the primary drop develops after only a short time ($t^*=0.1$) while, in contrast, for large $\mathscr{B}$ (= 5) a relatively large satellite forms from the narrow, tapered thread, but the satellite formation time is longer ($t^*=2.04$).

D. Effect of the capillary number $\mathscr{C}$

Figure 8 shows the (large) variation of the breaking time t_b as a function of the capillary number $\mathscr{C}$ with $\mathscr{B}=0.5$ and $\lambda=0.1$. We observe that t_b decreases significantly with increasing $\mathscr{C}$ for $\mathscr{C}<0.2$. However, for $\mathscr{C}>0.2$, decreases in the breaking time become gradual and t_b is nearly constant for $\mathscr{C}>0.75$. For $\mathscr{C}<0.2$ the drop grows slowly until it reaches the critical volume and the subsequent necking and breakup processes are relatively fast. In these cases, t_b is essentially determined by the time necessary for the drop fluid volume to reach the critical volume for detachment from the capillary tube. For large $\mathscr{C}$, accumulation of the drop fluid is fast and the critical volume is reached at earlier times. The accumulation time no longer determines the breaking time and, instead, the time for the subsequent necking and breakup process is most significant. We note that the necking and breaking process for large $\mathscr{C}$ is complicated because a large amount of the drop fluid exits the tube during the second stage and the fluid interface keeps extending and deforming. This breakup process is somewhat similar to that of a ''jetting'' flow, as shown in Fig. 8 for $\mathscr{C}=1$. For such

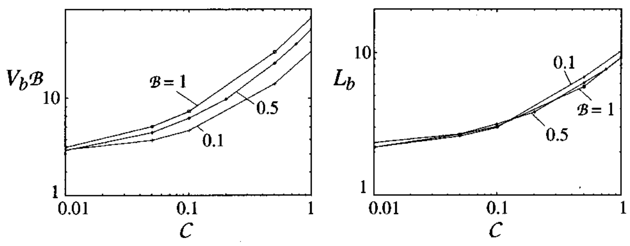

FIG. 9. Variation of L_b and V_b with $\mathscr{C}$ for $\lambda=0.1$ and three different Bond numbers, $\mathscr{B}=0.1$, 0.5, and 1.0.

large $\mathscr{C}$ flow conditions, the breakup time t_b primarily depends on the necking and breaking process in which the flow in the vicinity of the tube exit has a little influence: an approximately constant t_b is thus expected.

Figure 9 reports V_b and L_b as functions of the capillary number for $10^{-2}\leqslant\mathscr{C}\leqslant 1$, $\lambda=0.1$, and $\mathscr{B}=0.1$, 0.5, 1.0. Both L_b and V_b increase with $\mathscr{C}$. Since static analysis predicts $V_b\propto\mathscr{B}^{-1}$, this scaling is used in Fig. 9, and is seen to be useful for collapsing some of the data. In the cases studied, for fixed λ, the breaking length is only weakly dependent on $\mathscr{B}$ for a given $\mathscr{C}$.

As a final remark, when $\mathscr{C}\gg 1$ and the shape remains nearly spherical, the dimensionless drop volume scales as $V_d\propto(\mathscr{C}/\mathscr{B})^{3/4}$ as described by Wong *et al.*[12] (see also Ref. 5), who show that this result is in good agreement with their numerical calculations for $\lambda=0$ provided $\mathscr{C}/\mathscr{B}>10^3$. On the other hand, for $\lambda\gg 1$, long fluid columns form and Wilson's one-dimensional model[11] predicts $V_d=\sqrt{3}\pi(\mathscr{C}/\mathscr{B})^{1/2}+2.4/\mathscr{B}$. To study these asymptotic limits in detail would require more node points than used in our numerical simulations reported in the rest of the paper.

E. Effect of an external uniform flow

The above results summarize the response for a quiescent ambient fluid, $\mathbf{U}_\infty=\mathbf{0}$. In this last section, drop formation is studied for a uniform steady flow $\mathbf{U}_\infty$. The motivation for this flow configuration is to explore the possibility of controlling the drop size and the drop detachment rate. This idea was investigated numerically by Oguz and Prosperetti[21] in a study of bubble growth and detachment from a needle for the case of irrotational flow conditions and earlier research was summarized by Clift *et al.*[5] It has been observed that the external flow typically leads to the formation of smaller drops, which provides a useful control parameter since in the absence of flow the drop radius is proportional to the one-third power of the capillary tube radius. We now consider the low-Reynolds-number flow limit and summarize the change in drop volume, breakoff length, and breakoff time as the external flow velocity ($\mathscr{C}_{\rm out}$) is increased.

Figure 10 shows the interface shapes at breakup for different $\mathscr{C}$ and $\mathscr{C}_{\rm out}$ with other parameters fixed ($\mathscr{B}=0.5$ and $\lambda=0.1$). All of the results are shown with the same scale so that the drop size and the breakup length can be compared directly. The capillary numbers from top to bottom are $\mathscr{C}=10^{-2},10^{-1}$, and 1, and the outer capillary numbers, from

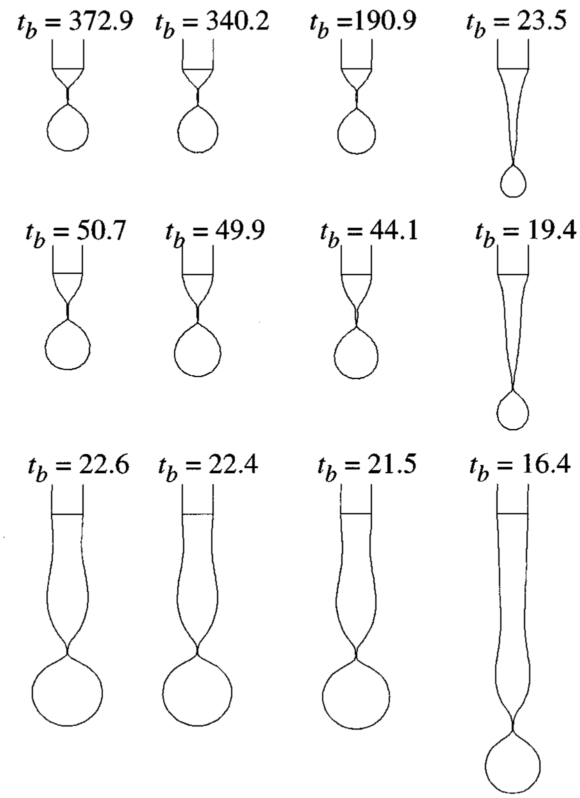

FIG. 10. Interface shapes at breakup for different $\mathscr{C}$ and $\mathscr{C}_{\rm out}$; $\mathscr{B}=0.5$ and $\lambda=0.1$. The capillary numbers $\mathscr{C}$, from top to bottom, are 10^{-2}, 10^{-1}, and 1, and the outer capillary numbers $\mathscr{C}_{\rm out}$, from left to right, are 0, 10^{-2}, 10^{-1}, and 1.

left to right, are $\mathscr{C}_{\rm out}=0,10^{-2},10^{-1}$, and 1. In each frame the dimensionless breakup time t_b is indicated. It is evident that imposing a constant flow on the ambient fluid can effectively influence the drop formation process, as indicated by Clift *et al.*[5] and quantified here for the viscous flow limit. As compared to the earlier cases of no externally imposed flow, with a constant $\mathbf{U}_\infty$, or finite $\mathscr{C}_{\rm out}$, a *smaller* primary drop, a longer breaking length L_b, and a shorter breaking time result, whereas, as discussed earlier, a larger $\mathscr{C}$ leads to a larger primary drop and a longer breaking length. For a given $\mathscr{C}$, the drag force on the drop fluid, which increases with increasing $\mathscr{C}_{\rm out}$, tends to stretch the fluid column, and the earlier breakup time therefore leads to the formation of a smaller primary drop. Figure 11 shows the variation of V_b as a function of $\mathscr{C}_{\rm out}$ ($\mathscr{B}=0.5$, $\lambda=0.1$, and $\mathscr{C}=0.1$).

In Fig. 10, it is observed that large values of $\mathscr{C}_{\rm out}$ not only alter the primary drop size and the breaking length, but also change the shapes of the interfaces dramatically (e.g., $\mathscr{C}_{\rm out}=1$ with $\mathscr{C}=10^{-2}$ and 10^{-1}). Thus we expect that the outer flow also influences the formation of satellite drops.

The influence of an applied flow on drop formation with different Bond numbers $\mathscr{B}$ is considered in Fig. 12, where the dimensionless drop volumes V_b at $\mathscr{C}_{\rm out}=0$ and 0.2 are compared for $\lambda=0.1$ and $0.1\leqslant\mathscr{B}\leqslant 5$. Significant differences in V_b are observed for small $\mathscr{B}$ (<0.1), but the differences are much smaller for $\mathscr{B}>O(1)$. There are now two forces trying to move the drop fluid away from the tube, one is the buoyancy force ($\mathscr{B}$) and the other is the viscous drag force

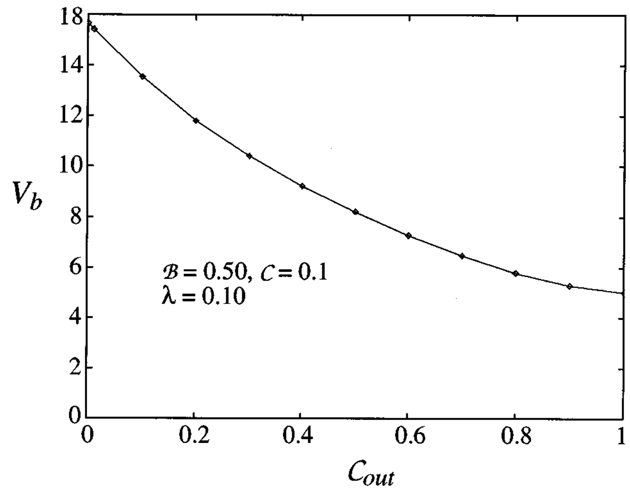

FIG. 11. Variation of V_b with $\mathscr{C}_{\rm out}$ for $\mathscr{B}=0.5$, $\lambda=0.1$, and $\mathscr{C}=0.1$.

exerted by the ambient fluid ($\mathscr{C}_{\rm out}$). The buoyancy force dominates for large Bond numbers, such as $\mathscr{B}=5$, which results in a rapid formation of the small primary drop ($t_b=5.32$). In contrast, for a small $\mathscr{B}=0.1$, the drag force exerted by the imposing flow is most significant.

Figure 13 provides a further view of interface shapes with $\mathscr{B}=0$, which is a limit of obvious relevance to micro-gravity applications. Two outer capillary numbers, $\mathscr{C}_{\rm out}=0$ and 0.2, are examined for $\lambda=0.1$ and $\mathscr{C}=0.1$. For $\mathscr{C}_{\rm out}=0$, as expected, the volume of the drop fluid increases continuously, the drop fluid remains attached to the tube, and the interface maintains a spherical shape due to interfacial tension. With an external flow, however, viscous stresses are exerted on the interface by the ambient fluid, and leads to drop breakup at $t_b=440.7$. It is interesting to note that a comparison of different simulations indicates that the interface shape for $\mathscr{B}=0$, $\mathscr{C}_{\rm out}=0.2$ (Fig. 13) is similar to that near breakup for $\mathscr{B}=0.1$, $\mathscr{C}_{\rm out}=0$ (Fig. 12).

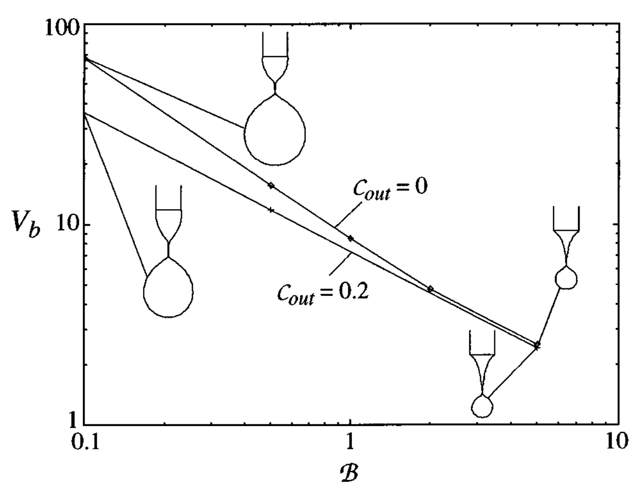

FIG. 12. Comparison of V_b for $\mathscr{C}_{\rm out}=0$ and $\mathscr{C}_{\rm out}=0.2$ with $\lambda=0.1$, $0.1\leqslant\mathscr{B}\leqslant 5$.

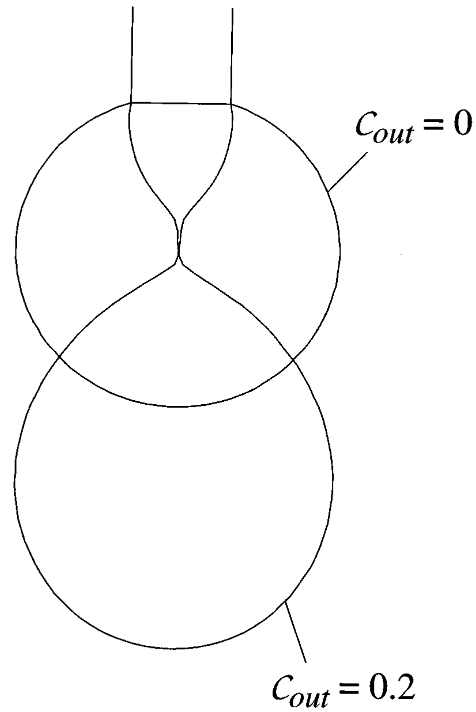

FIG. 13. Interface shapes for $\mathscr{C}_\infty=0,0.2$ with $\mathscr{B}=0$, $\lambda=0.1$, and $\mathscr{C}=0.1$.

IV. CONCLUDING REMARKS

We have studied numerically the dynamics of drop formation from a capillary tube for two-phase low-Reynolds-number flows. The emphasis has been on determining the volume of the primary drop as a function of the Bond number, capillary number, and the viscosity ratio. Known asymptotic limits have been summarized in the text and the figures reported here thus represent graphically, in the spirit of the compendium of Clift *et al.*[5] (Chap. 12), the complete dependence of the drop volume, breakup length, and breakup time as a function of the dimensionless parameters (which typically are outside the region where the asymptotic results are valid). The effect of an external flow, known to generally lead to smaller drop sizes, is here quantified for viscously dominated flows.

ACKNOWLEDGMENTS

We gratefully acknowledge financial support from the Petroleum Research Fund (Grant No. 28690-AC9). We also thank C. Maldarelli for supplying preprints of his research group's related studies. We thank M. P. Brenner for helpful conversations related to the generic problem of drop formation at capillaries.

APPENDIX

In this appendix we provide the details of the numerical implementation for the solution of the integral equations from which the boundary velocity is determined.

Given an initial shape for the interface, Eqs. (7a) and (7b) can be solved numerically by approximating the integral equations by a linear system of equations. Each boundary, S_D or S_T, is defined by a set of discrete boundary nodes at which the velocity is calculated. A hemispherical cap is assumed to be the initial shape of the drop at the end of the capillary and is represented by 15–20 points. With increases of the interface length, more points are added so as to preserve the numerical representation of the interface and the node points are uniformly redistributed along the interface every 5–10 time steps. For the calculations reported here the maximum number of node points is 100, which has been shown to be sufficient by performing several numerical simulations using more points. To resolve carefully smaller satellite drops than those studied here, more node points are necessary. Cubic splines are used for a continuous interpolation of the interface shape where the spline parameter is the arclength s along the interface measured from the corner of the tube exit at $z=0$ [i.e., $r(s)$, $z(s)$]. Along the capillary tube wall S_T $(r=1)$, the boundary is discretized using $r(z)$, a fixed number of points (20) are distributed along the capillary for a distance of 10 tube diameters and, beyond this point, the integral is truncated. For the unknown quantities (velocities and stress jumps), a linear piecewise interpolation in terms of the spline parameter between adjacent nodes is used.

The numerical integrations are performed with Gaussian quadratures using the IMSL Math/library routines. The absolute and relative error limits for the numerical integrations are chosen as 10^{-5} and 10^{-7}, respectively. Special care is required to handle the logarithmic singularity as $\mathbf{y}\rightarrow\mathbf{x}$. We subtract the logarithmic behavior of the singularity from the integrands and so reduce the integrands into a regular part and a singular part, whose contributions are computed separately (using different codes in the IMSL library). For most of the cases, the singular part $|\mathbf{x}-\mathbf{y}|$ is set to be 1% of the distance of the adjacent nodes. The resulting matrix equation is solved by iterative refinement. Once the linear system of equations is solved to obtain the interfacial velocities, the interface location is updated by solving the kinematic condition [Eq. (5)] using an explicit Euler method.

Numerical accuracy is assessed by increasing the boundary discretization and by monitoring the change of the drop fluid volume. Changing the boundary discretization is performed by increasing the node number, N, while keeping $\Delta t/\Delta s$ fixed, where Δt is the time step and Δs, proportional to $1/N$, is representative of the node spacing. The volume of the drop at the end of the computations is calculated numerically and compared with the sum of the initial volume and the fluid volume that flowed from the capillary tube during the computing time. The volume differences are always within 2% of the initial volume.

[1]W. J. Heideger and M. W. Wright, ''Liquid extraction during drop formation: Effect of formation time,'' AIChE. J. **32**, 1372 (1986).

[2]T. W. Shield, D. B. Bogy, and F. E. Talke, ''Drop formation by DOD ink-jet nozzles: A comparison of experiment and numerical simulation,'' IBM J. Res. Dev. **31**, 96 (1987).

[3]K. M. Sutherland, D. T. Derek, and L. S. Gordon, ''Independent control of blood gas PO_2 and PCO_2 in a bubble oxygenator,'' Clin. Phys. Physiol. Meas. **9**, 97 (1988).

[4]W. M. Sluyter, P. C. Slooten, C. A. Coprajj, and A. K. Chesters, ''The departure size of pool-boiling bubbles from artificial cavities at moderate and high pressure,'' Int. J. Multiphase Flow **17**, 153 (1991).

[5]R. Clift, J. R. Grace, and M. E. Weber, *Bubbles, Drops, and Particles* (Academic, New York, 1978).

[6]R. Kumar and N. R. Kuloor, ''The formation of bubbles and drops,'' Adv. Chem. Eng. **8**, 256 (1970).

[7]D. H. Michael, ''Meniscus stability,'' Annu. Rev. Fluid Mech. **13**, 189 (1981).

[8]S. Middleman, *Modeling Axisymmetric Flows: Dynamics of Films, Jets, and Drops* (Academic, New York, 1995).

[9]G. F. Scheele and B. J. Meister, ''Drop formation at low velocities in liquid-liquid systems: Part I. Prediction of drop volume,'' AIChE. J. **14**, 9 (1968).

[10]P. M. Heertjes, L. H. de Nie, and H. J. de Vries, ''Drop formation in liquid-liquid systems I. Prediction of drop volumes at moderate speed of formation,'' Chem. Eng. Sci. **26**, 441 (1971).

[11]S. D. Wilson, ''The slow dripping of a viscous fluid,'' J. Fluid Mech. **190**, 561 (1988).

[12]H. Wong, D. Rumschitzki, and C. Maldarelli, ''Theory and experiment on the low Reynolds number expansion, contraction and detachment of a bubble pinned at the tip of a submerged capillary'' (unpublished).

[13]J. Eggers and T. F. DuPont, ''Drop formation in a one-dimensional approximation of the Navier-Stokes equation,'' J. Fluid Mech. **262**, 205 (1994).

[14]J. Eggers, ''Theory of drop formation,'' Phys. Fluids **7**, 941 (1995).

[15]X. D. Shi, M. P. Brenner, and S. R. Nagel, ''A cascade of structure in a drop falling from a faucet,'' Science **265**, 219 (1994).

[16]M.P. Brenner, J. Eggers, K. Joseph, S. R. Nagel, and X. D. Shi, ''Breakdown of scaling in droplet fission at high Reynolds numbers,'' Phys. Fluids **9**, 1573 (1997).

[17]D. H. Peregrine, G. Shoker, and A. Symon, ''The bifurcation of liquid bridges,'' J. Fluid Mech. **212**, 25 (1990).

[18]D. Papageorgiou, ''Drop formation in a one-dimensional approximation of the Navier-Stokes equation,'' J. Fluid Mech. **262**, 205 (1994).

[19]M. P. Brenner, J. R. Lister, and H. A. Stone, ''Pinching threads, singularities and the number 0.0304 . . . ,'' Phys. Fluids **8**, 2827 (1996).

[20]J. Eggers, ''Nonlinear dynamics and breakup of free surface flows,'' Rev. Mod. Phys. **69**, 865 (1997).

[21]H. N. Oguz and A. Prosperetti, ''Dynamics of bubble growth and detachment from a needle,'' J. Fluid Mech. **257**, 111 (1993).

[22]R. Day and J. Hinch, ''Boundary integral simulation of a finite inviscid jet,'' in Proceedings of CFD95, Banff, Canada, edited by P. Thibault and D. Bergeron **2**, 375 (1995).

[23]M. S. Longuet-Higgins, B. R. Kerman, and K. Lunde, ''The release of air bubbles from an underwater nozzle,'' J. Fluid Mech. **230**, 365 (1991).

[24]X. Zhang and O. A. Basaran, ''An experimental study of dynamics of drop formation'' Phys. Fluids **7**, 1184 (1995).

[25]C. Pozrikidis, *Boundary Integral and Singularity Methods for Linearized Viscous Flow* (Cambridge University Press, Cambridge, England, 1992).

[26]J. Tanzosh, M. Manga, and H. A. Stone, ''Boundary integral methods for viscous free-boundary problems: Deformation of single and multiple fluid-fluid interfaces,'' *Proceedings of Boundary Element Technologies VII*, edited by C. A. Brebbia and M. S. Ingber (Computational Mechanics, Southampton, 1992), p. 19.

[27]S. H. Lee and L. G. Leal, ''The motion of a sphere in the presence of a deformable interface,'' J. Colloid. Interface Sci. **87**, 81 (1982).

[28]J. R. Lister, M. P. Brenner, and H. A. Stone, Presentation at the 1996 APS-DFD Meeting, Syracuse, NY (unpublished).